

THE IMPACT OF GALAXY FORMATION ON THE SUNYAEV-ZELOVICH EFFECT OF GALAXY CLUSTERS

DAISUKE NAGAI

Department of Astronomy and Astrophysics,
 Kavli Institute for Cosmological Physics,
 5640 S. Ellis Ave., The University of Chicago, Chicago IL 60637
 e-mail: daisuke@oddjob.uchicago.edu
 The *Astrophysical Journal*, submitted

ABSTRACT

We study the effects of radiative cooling and galaxy formation on the Sunyaev-Zel'dovich (SZ) observable-mass relations using high-resolution cosmological simulations. The simulations of eleven individual clusters spanning a decade in mass are performed with the shock-capturing eulerian adaptive mesh refinement N-body+gasdynamics ART code. To assess the impact of galaxy formation, we compare two sets of simulations performed in the adiabatic regime (without dissipation) and with radiative cooling and several physical processes critical to various aspects of galaxy formation: star formation, metal enrichment and stellar feedback. We show that the SZ signal integrated to sufficiently large fraction of the cluster volume correlates strongly with the enclosed cluster mass, regardless of the details of the cluster physics or dynamical state of the cluster. The slope and redshift evolution of the SZ flux-mass relation are also insensitive to the details of the cluster gas physics, and they are well characterized by the simple self-similar cluster model. While the tightness, slope and redshift evolution are relatively unaffected, we show that the radiative cooling and galaxy formation significantly modify the normalization of the SZ scaling relations. In our simulations, we find that the gas cooling and associated star formation suppress the normalization by $\approx 30 - 40\%$. The effect is due to the decrease in the hot gas fraction, which is offset slightly by the increase in the gas temperature. The baryon dissipation also causes the increase in the total cluster mass and modifies the normalization slightly. Finally, we show that the simulations that include gas cooling and star formation are in good agreement with the recent observational results on the SZ scaling relations obtained using 36 OVRO/BIMA SZ+Chandra X-ray cluster observations, while the simulations neglecting galaxy formation are inconsistent with the observed correlation. The comparison highlights the importance of galaxy formation in theoretical modelling of clusters and shows that the current generation of simulations produce clusters with gross properties quite similar to their observed counterparts.

Subject headings: cosmology: theory—clusters: formation—methods: numerical

1. INTRODUCTION

The Sunyaev-Zel'dovich (SZ) effect is a potentially powerful observational tool for cosmology. It is a small distortion in the cosmic microwave background (CMB) spectrum caused by scattering of CMB photons off a distribution of high energy electrons in dense structures such as clusters of galaxies (Sunyaev & Zeldovich 1970, 1972). This effect has a unique property that the signal is independent of redshift, making it particularly well suited for deep cluster surveys. Such surveys will be able to detect all clusters above a mass limit nearly independently of the redshift of the clusters (e.g., Holder et al. 2000; Weller et al. 2002). The next generation SZ instruments, such as the South Pole Telescope (SPT), should be capable of mapping a fairly large portion of the sky and finding $\gtrsim 10^4$ clusters with masses greater than $\approx 2 \times 10^{14} M_\odot$ independent of redshift (see the review by Carlstrom et al. 2002). Such a large and homogeneous sample of galaxy clusters will enable direct and precise measurements of the evolution of the number density of galaxy clusters as a function of redshift, and the expected survey yields will be sufficient to provide one of the most powerful constraints on the nature of dark energy (Wang & Steinhardt 1998; Haiman et al. 2001).

To realize the full statistical power of the upcoming

SZ surveys, however, the systematics would have to be controlled to the level comparable to the statistical uncertainty. One of the main sources of the systematics lies in the relation between the SZ observable and mass of clusters as a function of redshift. Making this connection is important because the mass of the cluster is not a direct observable. For the upcoming surveys, the requirement is to control the systematics in the SZ observable-mass relation to better than $\sim 5\%$ at all redshift (e.g., Carlstrom et al. 2002).

This poses a serious challenge to both observers and theorists. To date, observational studies of SZ scaling relations have been performed using two largest datasets of SZ measurements obtained by the OVRO/BIMA cm-wave imaging experiment (Cooray 1999; McCarthy et al. 2003; LaRoque 2005) and multiband SuZIE experiment (Benson et al. 2004) along with the X-ray observations. Recently, LaRoque (2005) analyzed the sample of 36 clusters observed with both OVRO/BIMA SZ and Chandra X-ray observations and showed that a tight correlation exists between the observed SZ flux and X-ray properties of clusters, such as X-ray temperature and derived total and gas masses of clusters. The observed regularity of the SZ clusters is an encouraging news, but further progress is clearly needed for the upcoming SZ surveys. The observational situation is expected to improve rapidly with

the advent of a number of dedicated SZ survey instruments, which will dramatically increase the sample size and the number of low-mass clusters.

On the theoretical side, a number of groups have studied the SZ scaling relations using semi-analytic models (Verde et al. 2002; McCarthy et al. 2003) and cosmological cluster simulations (Metzler 1998; White et al. 2002; da Silva et al. 2004; Diaferio et al. 2005; Motl et al. 2005). Motivated by the results of X-ray cluster observations in the past decade (see Voit 2005, for the review and references therein), the recent studies have focused on studying the impact of non-gravitational physical processes, such as gas cooling, star formation and energy feedback, on the SZ scaling relations. One of the main results is that the SZ signal integrated to sufficiently large fraction of the cluster volume is an extremely good proxy for the total cluster mass, independent of the details of the cluster gas physics or dynamical state of the cluster (see e.g., Motl et al. 2005). The slope and the redshift evolution of the SZ scaling relation also appear to be insensitive to the details of cluster gas physics (e.g., da Silva et al. 2004). While these results are encouraging for the cosmological applications, these previous studies used the large number of clusters extracted from large box cosmological simulations, and the resolution was inevitably limited to capture the relevant cluster physics. As such, the impact of galaxy formation on the normalization of the SZ scaling relations has not yet converged among different simulations. It is therefore important to push the theoretical modelling of SZ scaling relations and check the previous results using the high-resolution cluster simulations.

In this paper, we present such study using high-resolution simulations of eleven clusters designed to resolve the formation of cluster galaxies. Although the statistics is limited, these clusters span over a decade in mass and provide good leverage on the scaling relations. The mass resolution of our simulations is more than an order of magnitude higher than that in the previous studies. This work is therefore complimentary to the previous studies in the literature. Using these simulations, we study the impact of gas cooling and galaxy formation on the SZ scaling relations, including the normalization, slope and their redshift evolution. To test the predictions of the numerical simulation, we compare our results to the recent observational results on the SZ scaling relations for the sample of 36 clusters obtained using the OVRO+BIMA SZ and Chandra X-ray telescopes (LaRoque 2005).

The paper is organized as follows. In § 2 we define the observational quantities and present the relevant scaling laws predicted by the self-similar model. We describe the details of our simulations presented in this paper in § 3. In § 4 we present our main results and comparisons to the previous studies and the recent observational results. Finally, in § 5 we discuss our conclusions and their implications on the upcoming SZ cluster surveys.

2. THEORETICAL FRAMEWORK

2.1. Thermal Sunyaev-Zel'dovich Effect

The thermal SZ effect is a distortion in the CMB spectrum produced by the inverse Compton scattering of CMB photons off free electrons in dense structures such as clusters of galaxies. For a given line of sight, the

change in the CMB specific intensity caused by the thermal SZ effect at a frequency ν is given by $\Delta I_\nu/I_{\text{CMB}} = f_\nu(x)g_\nu(x)y$. The dimensionless comptonization parameter y is defined as,

$$y \equiv \frac{k_B\sigma_T}{m_e c^2} \int n_e(l) T_e(l) dl. \quad (1)$$

where n_e and T_e are the number density and temperature of the electrons, m_e is the electron rest mass, c is the speed of light, and σ_T is the Thomson cross-section. There are several frequency dependent factors, including $I_{\text{CMB}} = 2h\nu^3/c^2(e^x - 1)^{-1}$, $f_\nu(x) = [x(e^x + 1)/(e^x - 1) - 4](1 + \delta_{\text{SZ}}(x, T_e))$ and $g_\nu(x) = x^4 e^x/(e^x - 1)^2$, where $\delta_{\text{SZ}}(x, T_e)$ is the frequency dependent relativistic correction and $x \equiv h\nu/k_B T_{\text{CMB}}$. The corresponding change in the CMB temperature is given by $\Delta T_\nu/T_{\text{CMB}} = f_\nu(x)y$. In the Rayleigh-Jeans limit ($\nu \ll 200\text{GHz}$), $\Delta T_\nu/T_{\text{CMB}} = -2y$ and $\Delta I_\nu = (2k_B\nu^2/c^2)\Delta T_\nu$.

Let us now consider the SZ signal arising from a cluster located at redshift z . The SZ flux integrated over the solid angle of observation $d\Omega$ is given by $\Delta S_\nu = \int \Delta I_\nu d\Omega = I_{\text{CMB}} f_\nu(x) g_\nu(x) Y$, where Y is the integrated Compton-y parameter defined as

$$Y \equiv \int_\Omega y d\Omega = \frac{1}{d_A^2(z)} \left(\frac{k_B\sigma_T}{m_e c^2} \right) \int_V n_e T_e dV, \quad (2)$$

$d\Omega = dA/d_A^2(z)$ is the solid angle subtended on the sky, $d_A(z)$ is the angular diameter distance to the cluster at redshift z , and dA and dV are the area and volume of the cluster projected on the sky, respectively. Because Y depends on distance, we will work with the intrinsic thermal SZ signal, defined as

$$Y^{\text{int}} \equiv Y d_A^2(z) \propto f_{\text{gas}} M T_m. \quad (3)$$

Note that the integrated SZ flux is linearly sensitive to the gas mass $M_{\text{gas}} = f_{\text{gas}} M$ and mass-weighted temperature T_m of the cluster, where f_{gas} is the gas fraction and M is the total mass of the cluster.

2.2. Self-Similar scaling relations

In the absence of cooling and heating processes, clusters are expected to scale self-similarly (Kaiser 1986). The self-similar model predicts that the temperature of the gas scales with the cluster mass as

$$M \propto T^{3/2} E^{-1}(z) \quad (4)$$

where $M \equiv 4\pi r_\Delta^3 \Delta_c \rho_{\text{crit}}/3$ is the halo mass enclosed within r_Δ , defined as the radius of a spherical volume within which the mean density is Δ_c times the *critical density*, ρ_{crit} , at that redshift (Bryan & Norman 1998). The redshift evolution factor, $E(z)$, is related to the redshift-dependent Hubble parameter $H(z) = 100hE(z)$ $\text{km s}^{-1}\text{Mpc}^{-1}$ with $E^2(z) = \Omega_M(1+z)^3 + \Omega_\Lambda$ in the flat cosmology.

Inserting Eq. 4 into Eq. 3, we obtain the SZ scaling relation predicted by the self-similar model,

$$Y^{\text{int}} \propto \begin{cases} f_{\text{gas}} M^{5/3} E^{2/3}(z) \\ f_{\text{gas}} T^{5/2} E^{-1}(z) \end{cases} \quad (5)$$

3. SIMULATIONS

In this study, we analyze high-resolution cosmological simulations of eleven cluster-size systems in the “concordance” flat Λ CDM model: $\Omega_m = 1 - \Omega_\Lambda = 0.3$,

$\Omega_b = 0.04286$, $h = 0.7$ and $\sigma_8 = 0.9$, where the Hubble constant is defined as $100h \text{ km s}^{-1} \text{ Mpc}^{-1}$, and σ_8 is the power spectrum normalization on $8h^{-1} \text{ Mpc}$ scale. The simulations were done with the Adaptive Refinement Tree (ART) N -body+gasdynamics code (Kravtsov 1999; Kravtsov et al. 2002), a Eulerian code that uses adaptive refinement in space and time, and (non-adaptive) refinement in mass (Klypin et al. 2001) to reach the high dynamic range required to resolve cores of halos formed in self-consistent cosmological simulations.

To set up initial conditions we first ran a low resolution simulation of $80h^{-1} \text{ Mpc}$ and $120h^{-1} \text{ Mpc}$ boxes and selected eleven clusters with the masses ranging from $M_{500c} \approx 3.5 \times 10^{13}$ to $9 \times 10^{14}h^{-1} \text{ M}_\odot$. The properties of clusters at the present epoch are listed in Table 1. The perturbation modes in the lagrangian region corresponding to the sphere of several virial radii around each cluster at $z=0$ was then re-sampled at the initial redshift, $z_i = 25$ for the three most massive clusters (CL1-3) and $z_i = 49$ for the remaining eight clusters in the sample. For the three most massive clusters we have resampled radius of $3R_{\text{vir}}(z=0)$, while for the rest of the clusters the resampling sphere had radius of $5R_{\text{vir}}(z=0)$, where $R_{\text{vir}}(z=0)$ is the virial radius enclosing overdensities of $\Delta_{\text{vir}} = 334$ with respect to the mean density of the universe at $z=0$. During the resampling we retained the previous large-scale waves intact but included additional small-scale waves, as described by Klypin et al. (2001). The resampled lagrangian region of each cluster was then re-simulated with high dynamic range.

High-resolution simulations were run using 128^3 uniform grid and 8 levels of mesh refinement in the computational boxes of $120h^{-1} \text{ Mpc}$ for CL1-CL3 and $80h^{-1} \text{ Mpc}$ for CL4-CL11, which corresponds to the dynamic range of $128 \times 2^8 = 32768$ and peak formal resolution of $80/32, 768 \approx 2.44h^{-1} \text{ kpc}$, corresponding to the actual resolution of $\approx 2 \times 2.44 \approx 5h^{-1} \text{ kpc}$. Only the region of $\approx 3 - 10h^{-1} \text{ Mpc}$ around the cluster was adaptively refined, the rest of the volume was followed on the uniform 128^3 grid. The mass resolution corresponds to the effective 512^3 particles in the entire box, or the Nyquist wavelength of $\lambda_{\text{Ny}} = 0.469h^{-1}$ and $0.312h^{-1}$ comoving megaparsec for CL1-3 and CL4-11, respectively, or $0.018h^{-1}$ and $0.006h^{-1} \text{ Mpc}$ in the physical units at the initial redshift of the simulations. The dark matter particle mass in the region around the cluster was $9.1 \times 10^8h^{-1} \text{ M}_\odot$ for CL1-3 and $2.7 \times 10^8h^{-1} \text{ M}_\odot$ for CL4-CL11, while other regions were simulated with lower mass resolution.

As the zeroth-level fixed grid consisted of only 128^3 cells, we started the simulation already pre-refined to the 2nd level ($l = 0, 1, 2$) in the high-resolution lagrangian regions of clusters. This is done to ensure that the cell size is equal to the mean interparticle separation and all fluctuations present in the initial conditions are evolved properly. During the simulation, the refinements were allowed to the maximum $l = 8$ level and refinement criteria were based on the local mass of DM and gas in each cell. The logic is to keep the mass per cell approximately constant so that the refinements are introduced to follow the collapse of matter in a quasi-lagrangian fashion. For the DM, we refine the cell if it contains more than two dark matter particles of the highest mass resolution specie. For gas, we allow the mesh refinement, if the cell

contains gas mass larger than four times the DM particle mass scaled by the baryon fraction. In other words, the mesh is refined if the cell contains the DM mass larger than $2(1 - f_b)m_p$ or the gas mass larger than $= 4f_b m_p$ (where m_p is given above and $f_b = \Omega_b/\Omega_m = 0.1429$). We analyze clusters at the present-day epoch as well as their progenitors at higher redshifts.

We repeated each cluster simulation with and without radiative cooling. The first set of “adiabatic” simulations have included only the standard gasdynamics for the baryonic component without dissipation and star formation. The second set of simulations included gasdynamics and several physical processes critical to various aspects of galaxy formation: star formation, metal enrichment and thermal feedback due to the supernovae type II and type Ia, self-consistent advection of metals, metallicity dependent radiative cooling and UV heating due to cosmological ionizing background (Haardt & Madau 1996). We will use labels ‘ad’ and ‘csf’ for the adiabatic simulations and simulations with cooling and star formation, respectively.

The cooling and heating rates take into account Compton heating and cooling of plasma, UV heating, atomic and molecular cooling and are tabulated for the temperature range $10^2 < T < 10^9 \text{ K}$ and a grid of metallicities, and UV intensities using the Cloudy code (ver. 96b4, Ferland et al. 1998). The Cloudy cooling and heating rates take into account metallicity of the gas, which is calculated self-consistently in the simulation, so that the local cooling rates depend on the local metallicity of the gas. Star formation in these simulations was done using the observationally-motivated recipe (e.g., Kennicutt 1998): $\dot{\rho}_* = \rho_{\text{gas}}^{1.5}/t_*$, with $t_* = 4 \times 10^9 \text{ yrs}$. The code also accounts for the stellar feedback on the surrounding gas, including injection of energy and heavy elements (metals) via stellar winds and supernovae and secular mass loss. The detailed description and implementation of the star formation and stellar feedback are provided in Kravtsov et al. (2005).

The high-resolution and the inclusion of various physical processes critical to galaxy formation enable unique studies of the impact of galaxy formation on the properties of the ICM. The mass resolution of the simulation is sufficiently high to resolve the galactic-size halos as small as $1/10,000$ of the mass of the host cluster (Nagai & Kravtsov 2005), and the observed properties of the cluster galaxies are well reproduced in the current simulations (Nagai et al. 2005b, in preparation). These simulations have been used to study the effects of galaxy formation on the gas fractions in clusters (Kravtsov et al. 2005). The main results of this paper is that gas cooling and star formation significantly suppress the gas fraction within the virial radius of the cluster. The comparisons of the simulations to the recent deep Chandra X-ray observations of nearby clusters further showed that the current simulations reproduce the observed gas fractions remarkably well (Kravtsov et al. in preparation). Because the SZ signal is proportional to the cluster gas fraction, these results indicate that the impact of galaxy formation on the SZ flux may also be significant.

Throughout this paper we use estimates of Y^{int} , mass and other cluster observables within different commonly used radii, defined by the total matter overdensity they

TABLE 1
SIMULATED CLUSTER SAMPLE OF THE CSF RUN AT $z=0$

Name	R_{500c}	M_{500c}^{gas}	M_{500c}^{tot}	$\langle T_{\text{spec}} \rangle$
	$h^{-1}\text{Mpc}$	$h^{-1}10^{13} M_{\odot}$	$h^{-1}10^{14} M_{\odot}$	keV
CL1	1.160	8.19	9.08	10.0
CL2	0.976	5.17	5.39	8.1
CL3	0.711	1.92	2.09	4.1
CL4	0.609	1.06	1.31	2.7
CL5	0.661	1.38	1.68	3.9
CL6	0.624	1.22	1.41	3.2
CL7	0.522	0.74	0.82	1.7
CL8	0.487	0.43	0.67	2.2
CL9	0.537	0.78	0.90	2.2
CL10	0.509	0.62	0.77	2.1
CL11	0.391	0.27	0.35	1.2

enclose. We will use radii r_{2500} , r_{500} , r_{200} enclosing overdensities of $\Delta_c = 2500$, 500, and 200 with respect to the critical density, ρ_{crit} , as well as radii r_{180} and r_{vir} enclosing overdensities of $\Delta_m = 180$ and Δ_{vir} with respect to the mean density of the universe. The latter is equal to $\Delta_{\text{vir}} \approx 334$ at $z=0$ and ≈ 200 at $z=1$ for the cosmology adopted in our simulations. The virial radius and masses of clusters within r_{500c} for the CSF run at $z=0$ are given in Table 1. For reference, we also give the spectral X-ray temperature, $\langle T_{\text{spec}} \rangle$, of individual clusters extracted from the mock Chandra analysis (Nagai et al. 2005, in preparation). The spectral temperature, $\langle T_{\text{spec}} \rangle$, is equivalent to the single-temperature fit to the total cluster spectrum in the radial range $70 \text{ kpc} < r < r_{500c}$.

4. RESULTS

In this section, we study the impact of gas cooling and galaxy formation on the SZ scaling relations using the cosmological cluster simulations. Our general strategy is to assess the effects of various physical processes on the cluster observables and the scaling relations by comparing the simulations with and without radiative cooling and star formation.

4.1. Pressure Profiles

Since the SZ effect is sensitive to the pressure of the ICM, we will start with the analysis of the pressure profiles. Figure 1 shows the comparisons of the mean pressure profiles at $z=0$ and $z=1$ for our entire sample of clusters simulated in the adiabatic regime and with gas cooling and star formation. To compute the mean profiles, we first normalize the differential and cumulative pressure profiles of individual clusters using the mean integrated pressure within the sphere of r_{500c} , denoted as \bar{P}_{500c} , and plot them as a function of the cluster-centric radius in units of r_{500c} . The mean profiles are computed by averaging the normalized profiles over the entire cluster sample. To highlight the impact of gas cooling and star formation on the pressure profiles, we normalize the profiles of the CSF run using \bar{P}_{500c} of the adiabatic run

for each cluster. The shaded bands show the 1σ rms scatter around the mean profile of the CSF run. The mean and scatter of the profiles are computed for the logarithm of pressure.

The Figure shows that the simulated clusters ranging in an order of magnitude in mass show remarkably similar pressure profiles at all radii. The differential pressure profile declines by nearly four orders of magnitude from the center to r_{500c} , and the scatter is small ($\approx 20\%$) throughout the cluster. In the outskirts of the cluster, the rate of decline is generally faster than that of the gas density profile and the gravitationally dominant dark matter. This is because the pressure is the product of the gas density and temperature for the ideal gas, and the latter also declines with radius (see Mottl et al. 2005; Vikhlinin et al. 2005b). For example, the typical power-law slope of the differential pressure profile is ≈ -3.5 at r_{500c} , which is steeper than the typical slope of the density profile of ≈ -3 seen in the cosmological simulations (Navarro et al. 1996, 1997) as well as the recent X-ray observations (Vikhlinin et al. 2005a).

One of the main results from this analysis is that the pressure is suppressed throughout the cluster in the CSF runs compared to the adiabatic runs. The cumulative pressure at r_{500c} , for example, is suppressed by $\approx 25\%$ on average, and this effect is relatively constant ($\approx 25\text{--}35\%$) in the region outside $> 0.2r_{500c}$ at $z=0$. In the cluster center, the pressure is significantly more concentrated, and its profile becomes steeper, because the potential is deeper and the density profile is steeper due to the baryon dissipation and the contraction of dark matter (Gnedin et al. 2004). Note, however, that this high pressured cluster core contributes very little to the cumulative pressure at large radii. For example, the inner regions within $< 0.1r_{500c}$ contributes less than 2% of the total SZ signal within r_{500c} . Thus, the SZ signal integrated out to a sufficiently large radius is insensitive to the gas properties in the cluster core.

Although the general trends are similar, the suppression of pressure varies more strongly with radius at $z=1$, because a dense, cool core dominates the larger fraction of r_{500c} at high redshift. Nevertheless, we find that the suppression of the cumulative pressure at r_{500c} is comparable at $z=0$ and 1. However, the difference becomes more apparent in the inner regions; for example, the effect at r_{2500c} changes from 35% at $z=0$ to 20% at $z=1$. If a similar trend exists in real clusters this implies that the redshift evolution of the SZ scaling relation is expected to deviate from the prediction of the self-similar model, if the SZ flux is computed within the aperture considerably smaller than r_{500c} .

In order to better understand the suppression of the pressure profile, we examine the impact of gas cooling and star formation on the gas density, temperature and entropy profiles. The Figure 2 shows that the suppression of the pressure is accompanied by the strong suppression in the gas density and the moderate increase in the gas temperature. The entropy profile provides further insights into these phenomena, because it uniquely characterizes the pressure, gas density and temperature profiles of the ICM, given the shape of its confining potential well (see Voit et al. 2002 and references therein). The Figure 2 shows that the entropy of gas, defined as

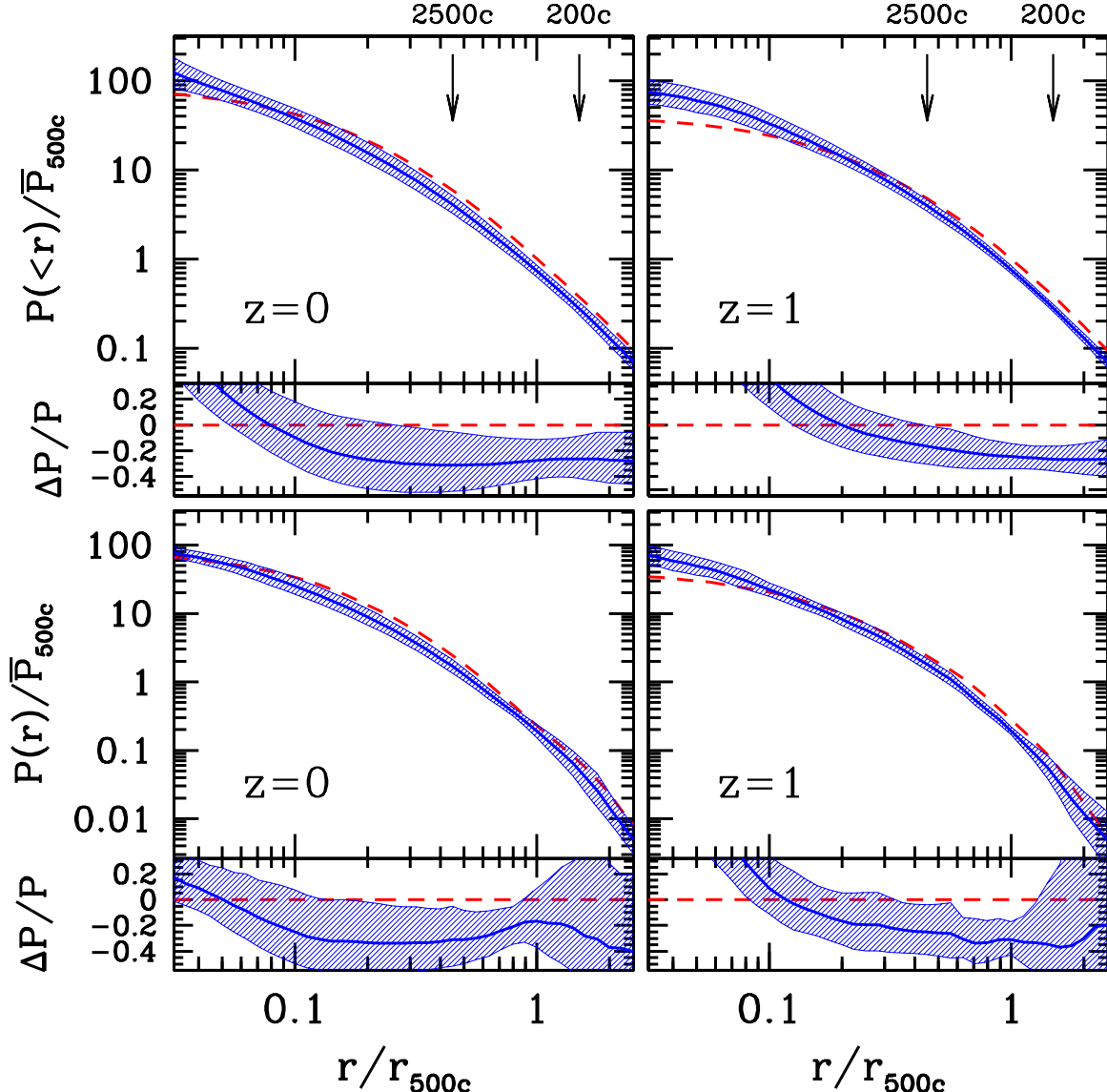


FIG. 1.— Cumulative (top panels) and differential (bottom panels) pressure profiles for the eleven clusters used in our analysis at $z=0$ (left column) and $z=1$ (right column). The dashed lines show the mean profiles in the adiabatic simulations averaged over eleven clusters. The solid lines show the mean profiles in the simulations with cooling and star formation. Note that all profiles are normalized to the mean cumulative pressure at r_{500c} in the adiabatic runs, \bar{P}_{500c} , at each epoch. The bottom panel of each figure shows the fractional deviation of the mean profile of the CSF run relative to the mean profile of the adiabatic run. In all panels, the shaded bands show the 1σ rms scatter around the mean for the eleven clusters. The vertical arrows in the top panels show the radii enclosing overdensities of 2500 and 200 with respect to the critical density at each epoch.

$S \equiv T/n^{2/3}$, is enhanced throughout the cluster out to $2 \times r_{500c}$. The effect peaks around $0.3r_{500c}$, and the entropy is enhanced by about 40% at r_{500c} . In our simulations, gas cooling and star formation can increase the entropy of gas in one of two ways: (1) the high entropy gas from outside flows in to replenish the gas removed by gas cooling and star formation in the inner region (Voit & Bryan 2001) or (2) the direct heating of the ICM by the energy injection from supernova explosions. The former is likely a dominant mechanism that shapes the overall entropy distribution, while the second process is important for regulating the rate of gas cooling in the high density region (e.g., the vicinity of the central galaxy and the cluster galaxies), where stars are forming with

sufficiently high rate.

To examine the mass dependence of the effects, we split the sample in half and show the mean profiles of the six most massive and five least massive clusters in the Figure 2. The Figure shows that the shape and the normalization of the pressure profiles exhibit the smallest systematic trend with mass. In the outskirt of the clusters $> 0.3r_{500c}$, we find similarly small systematic trend with mass for the gas density, temperature and entropy profiles. In the inner region, on the other hand, we find slightly more pronounced mass dependence in all profiles. Among them, the pressure profile shows the smallest trend with mass. In less massive clusters, we find that the changes in gas density and temperature be-

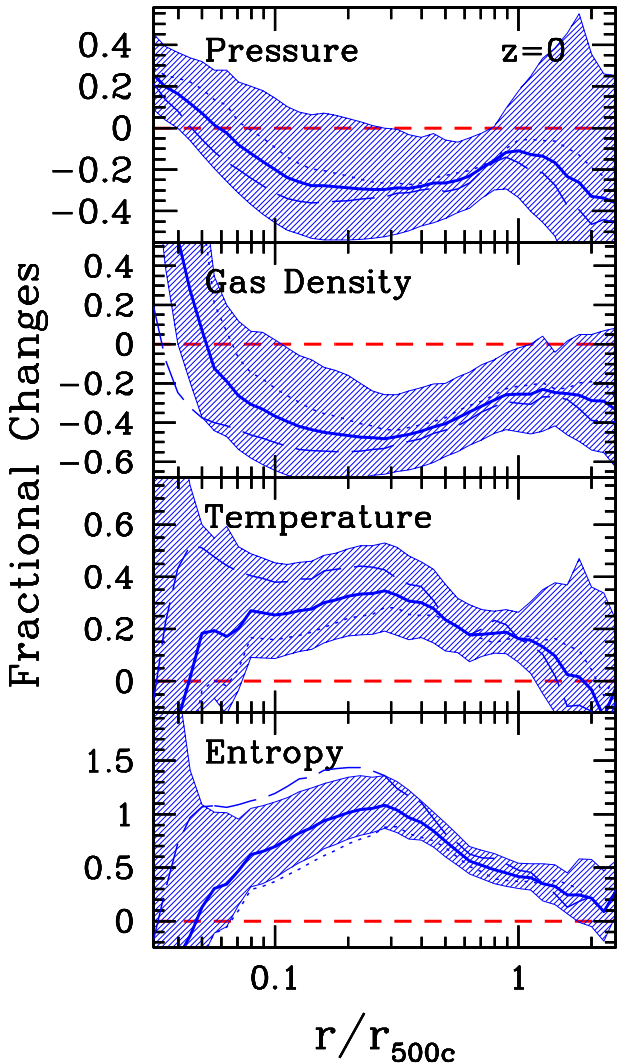


FIG. 2.— Impact of gas cooling and star formation on the pressure, gas density, temperature and entropy profiles (from top to bottom) of the simulated clusters at $z=0$. The *solid* lines show the fractional changes of the mean differential radial profiles in the CSF simulations averaged over eleven clusters relative to the mean profiles in the adiabatic runs, indicated by the line at zero. The *dotted* and *dashed* lines show the same for the subsamples of six most and five least massive clusters in our sample, respectively. Note that the mean profile of each quantity is computed by first normalizing the profiles of each cluster by the value of the cumulative profile at r_{500c} and averaging these normalized profiles over the samples.

come larger. Since the signs of these changes are opposite, these effects cancel each other to give the smallest mass dependence on pressure. In contrast, the effects add constructively to give the largest mass dependence of entropy.

The main conclusion from this analysis is that the cooling and star formation suppress the amplitude of the gas pressure and therefore the SZ signal, and the effect depends rather weakly on the mass of the cluster. These results imply that the processes of galaxy formation will modify the normalization of the SZ flux-mass relation, but its impact on the slope of the relation is expected to be small. This is the main topic of the discussion in the next section.

4.2. The SZ scaling relations

We will start with the SZ flux-total mass (SZ-M) relation because this is the relation directly relevant for the cosmological application. Figure 3 shows the comparison of the SZ-total mass scaling relation at r_{500c} and its redshift evolution for the sample of eleven clusters in the adiabatic and CSF runs. At each epoch, we performed the fits to the entire sample of simulated clusters using a simple power-law relation,

$$Y = A_{14} \times 10^{-6} \left(\frac{M}{10^{14} h^{-1} M_{\odot}} \right)^{\alpha_M}, \quad (6)$$

where A_{14} is the normalization at $10^{14} h^{-1} M_{\odot}$ in units of 10^{-6} and α_M is the slope. In practice, we fit a straight line to the $\log(Y)$ - $\log(M)$ relation by minimizing the χ^2 . The values of the best-fit normalization and slope measured at different radii, including r_{180m} , r_{vir} , r_{200c} , r_{500c} and r_{2500c} , are listed in Table 2. The values in the adiabatic simulations are marked 'ad', while those in the simulations with cooling and star formation are marked 'csf' (e.g., A_{14}^{csf}). The best-fit parameters in the Table and the right panel of the Figure 3 are obtained by fitting the normalization and slope simultaneously. To highlight any deviation from the self-similar slope, the best-fit relations shown in the left panel of the Figure 3 are obtained by fixing the slope to $5/3$. Note that fitting for the slope changes the best-fit normalization by no more than 5% at both $z=0$ and $z=1$.

In the right panel of the Figure 3, the errorbars indicate 2σ confidence region of the best-fit slope and normalization in the CSF simulations at each epoch. Since the redshift evolution of the normalization is measured relative to the relation at $z=0$, the errorbars at $z>0$ include the uncertainties in the best-fit normalizations at each epoch and $z=0$ added in quadrature. Note also that the sizes of the errorbars are comparable for the adiabatic simulations. The errorbars shown in the Figures 5 and 6 are also computed in the same way.

The left panel shows that the SZ signal integrated within the sphere of r_{500c} correlates very strongly with the enclosed cluster mass at both $z=0$ and 1. The rms scatter is about 10-15% in both adiabatic and cooling runs. Moreover, we find that the slope of the adiabatic run is in very good agreement with the predicted slope of the self-similar model. The best-fit slope of the CSF run is also not very different from the predicted slope of $5/3$, but there is an indication that the slope may be systematically steeper by $\lesssim 0.1$. Unfortunately, however, the current sample size is too small to rule out the predicted slope of the self-similar model with statistical significance. A larger sample of simulated clusters is clearly needed to assess this effect in the future studies.

While the tightness and the slope of the relations are relatively unaffected, gas cooling and star formation significantly modify the normalization of the SZ-total mass relation. Compared to the adiabatic run, the normalization of the CSF run is lower by 41, 34 and 27% at r_{2500c} , r_{500c} and r_{180m} .

The right panel shows that the redshift evolution of the SZ-total mass relation is consistent with the prediction of the self-similar model in the entire redshift range considered here. First, the slope is constant with redshift. Second, the redshift evolution of the normalization is in

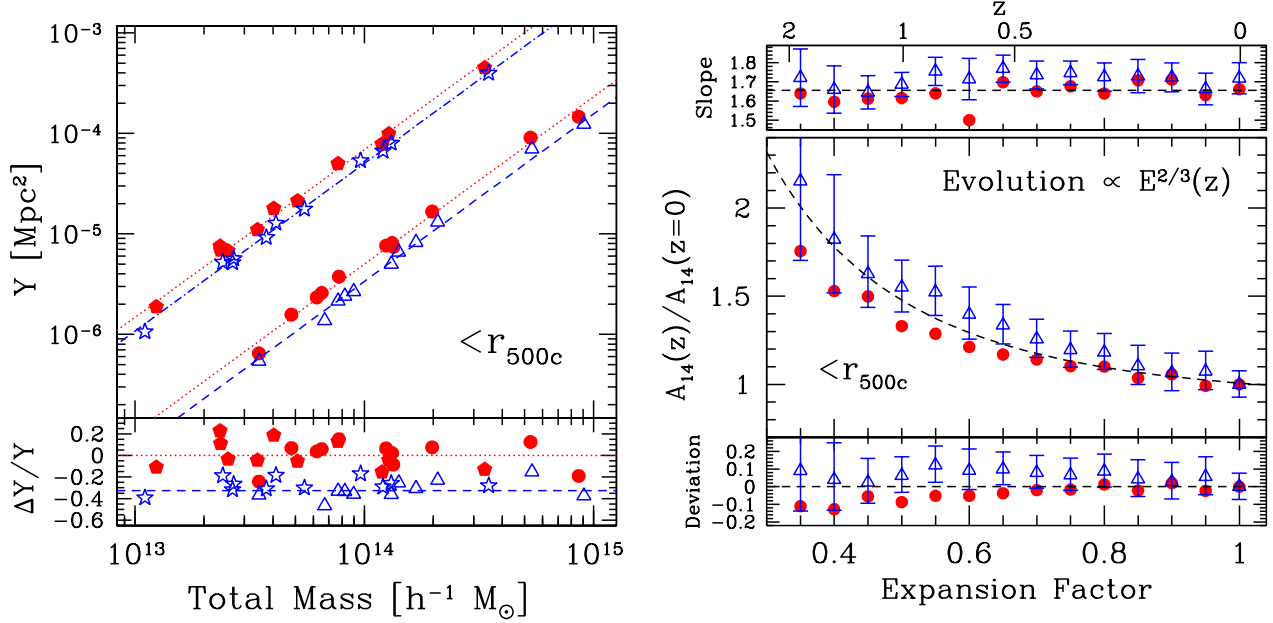


FIG. 3.— The SZ flux-total mass relations for the eleven clusters in the adiabatic (solid symbols) and cooling (open symbols) simulations. *Left-top panel*: the relation between the integrated compton-Y vs. total mass enclosed within the sphere of radius r_{500c} at $z=0$ (bottom lines and points) and $z=1$ (top lines and points). The solid circles and solid pentagons are the adiabatic runs at $z=0$ and 1, while the open triangles and open stars are the cooling runs at these epochs, respectively. At each epoch, the dotted and dashed lines show the best-fit relations for the adiabatic and cooling runs with the slope fixed at the self-similar value of 5/3. For clarity, the $z=1$ relations are shifted upward by a factor of ten. *Left-bottom panel*: the fractional deviation of individual clusters from the best-fit relation of the adiabatic runs at each epoch. The dashed line indicates the best-fit relation of the cooling runs at $z=0$. *Right panel*: the redshift evolution of the slope (top) and the normalization (middle) of the SZ flux-total mass relation between $z=2$ and the present day. The solid circles and open triangles indicate the adiabatic and cooling runs, respectively. The dashed lines indicate the slope of 5/3 (top) and the evolution of normalization predicted by the self-similar model (middle). The errorbars indicate 2σ confidence region of the best-fit slope and normalization in the CSF runs at each epoch. The bottom panel shows the fractional deviation of the best-fit normalization from the self-similar prediction as a function of time.

good agreement with the predicted evolution of the self-similar model. We also find similar results at other radii considered in this paper.

To better understand the impact of galaxy formation on the SZ scaling relation, we also examine their effects on f_{gas} and T_m in the Figure 4. Compared to the adiabatic run, we find that f_{gas} is lower by 38% in the CSF run; however, its effect on the SZ flux is offset partially by the increase in T_m by 9%. The net effect is the reduction of the SZ signal by 32%, which falls slightly short of the 34% change in the normalization of the SZ-M relation. This illustrates that the changes in f_{gas} and T_m alone do not fully account for the change in the normalization.

In addition, we find that the baryon dissipation slightly modifies the total mass of the cluster (see also Kravtsov et al. 2005, in preparation). Our simulations show that the median increase in M_{tot} at r_{500c} is about 5%. The effect becomes larger at the smaller radii, and it is about 20% at r_{2500c} . This effect will cause the shift in the SZ-M relation in both x- and y-directions by the same amount. However, since the slope of the relation is $\approx 5/3$, the 5% shift in the positive x-axis translates into the 8% shift in the negative y-axis. The net effect is therefore the negative 3% change in the normalization due to the change in M_{tot} . Putting them all together, we find that the 34% decrease in the normalization of the SZ-M relation

at r_{500c} is due to the combined effects of 38% decrease in f_{gas} , 9% increase in T_m and the net 3% decrease due to the change in M_{tot} . Note also that the inclusion of gas cooling and star formation causes decrease in the SZ signal and M_g within r_{500c} by 29% and 35%, respectively.

Finally, we check the redshift evolution of f_{gas} and T_m . The self-similar model predicts that f_{gas} is constant with time, while T_m of a given mass evolves with time according to the Eq. 4. To examine the deviation from the predicted evolution, the Figure 5 plots the deviation of the best-fit normalization of the $f_{gas} - M$ and $T_m - M$ relations at $M_{500c} = 10^{14} h^{-1} M_\odot$ from the predicted evolution as a function of redshift. The Figure shows that f_{gas} and T_m of a given mass in the CSF runs deviate from the predicted evolution of the self-similar model, while the evolution in the adiabatic runs is consistent with the self-similar model. In the CSF runs, the deviation increases toward higher redshifts. On average, f_{gas} is higher by about 12% at $z=1$ and 17% at $z=2$ compared to its value at $z=0$, while T_m is lower by an almost equal amount at each epoch. Since the SZ signal is linearly proportional to both of these quantities, the evolution in f_{gas} is canceled almost exactly by the evolution in T_m . Note also that we did not find systematic evolution in the impact of the baryon dissipation on the total mass with redshift. This explains why the SZ signal of a given mass shows very little evolution beyond the evolution predicted by the self-similar model.

TABLE 2
THE NORMALIZATION AND SLOPE OF THE SZ SCALING RELATIONS AT $z=0$

Δ	SZ-Total Mass				SZ-Gas Mass				SZ-Temperature			
	A_{14}^{ad}	α_M^{ad}	A_{14}^{csf}	α_M^{csf}	A_{13}^{ad}	$\alpha_{M_g}^{\text{ad}}$	A_{13}^{csf}	$\alpha_{M_g}^{\text{csf}}$	A_5^{ad}	α_T^{ad}	A_5^{csf}	α_T^{csf}
180m	2.59	1.63	1.88	1.68	1.55	1.63	2.19	1.60	18.24	2.52	12.06	2.60
vir	3.11	1.61	2.20	1.67	1.86	1.61	2.61	1.60	14.11	2.52	9.18	2.63
200c	3.78	1.62	2.56	1.70	2.29	1.62	3.24	1.60	9.98	2.50	6.37	2.62
500c	4.99	1.66	3.29	1.73	3.08	1.65	4.59	1.60	5.97	2.45	3.63	2.61
2500c	8.82	1.68	5.22	1.77	6.31	1.64	9.27	1.58	2.10	2.50	1.19	2.73

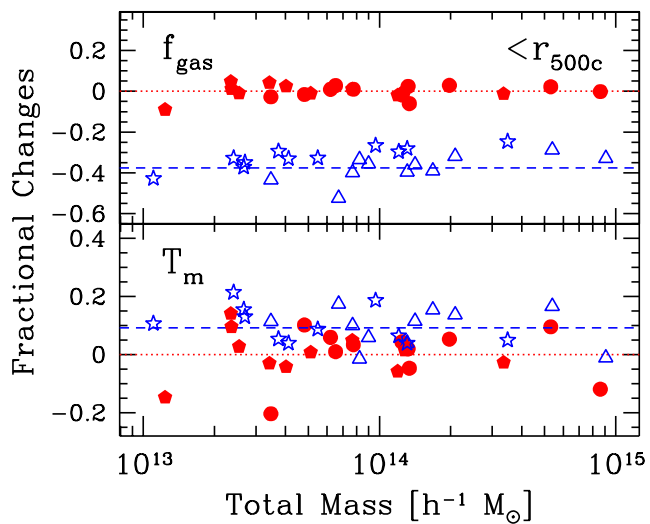


FIG. 4.— Fractional changes in the gas mass fraction (top) and mass-weighted temperature (bottom) enclosed within the sphere of radius r_{500c} between the adiabatic and CSF simulations as a function of cluster mass. The solid circles and solid pentagons are the adiabatic runs at $z=0$ and 1, while the open triangles and open stars are the cooling runs at these epochs, respectively. The fractional deviation of the gas mass fractions in the individual clusters from the mean gas mass fraction of the adiabatic runs at each epoch, indicated by the dotted line at zero. The dashed line indicates the best-fit relation of the cooling runs at $z=0$.

So far, we have focused on the SZ-total mass relation because of its direct relevance for the cosmological studies. Unfortunately, however, the cluster mass is not a direct observable, and making the unbiased measurements of the SZ-M relation is difficult in practice. Therefore, it is also useful to study the relations between the SZ signal and the global properties of clusters that can be measured more reliably from the observations. This can provide a useful direct test of the simulations.

Here, we consider two such quantities, including the gas mass, M_g , and mass-weighted temperature, T_m , of the cluster. Figure 6 shows the SZ- M_g and SZ- T_m relations at r_{500c} and the redshift evolution of their slope and normalization. At each timestep, we perform the fits to the entire sample of simulated clusters using the

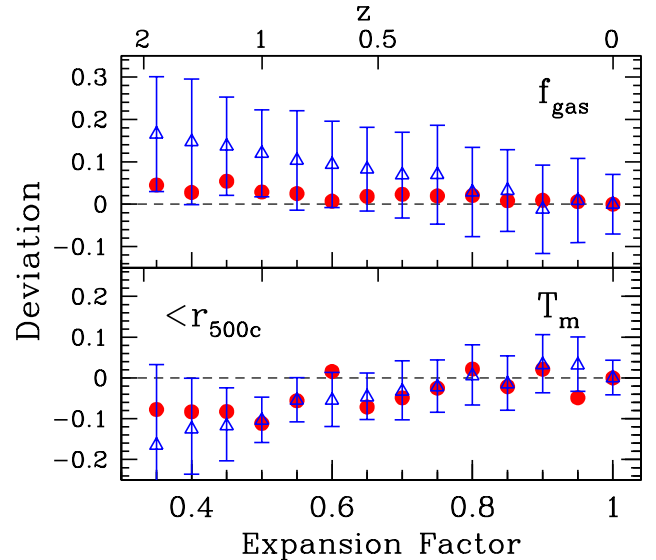


FIG. 5.— The evolution of the gas mass fraction (top) and mass-weighted temperature (bottom) at $M_{500c} = 10^{14} h^{-1} M_\odot$. The fractional deviation of the best-fit normalization from the self-similar prediction, indicated by the dashed line. The errorbars indicate 2σ statistical uncertainties in the CSF runs at each epoch.

following simple power-law relations,

$$Y = A_{13} \times 10^{-6} \left(\frac{M_g}{10^{13} h^{-1} M_\odot} \right)^{\alpha_{M_g}} \quad (7)$$

$$Y = A_5 \times 10^{-5} \left(\frac{T_m}{5 \text{ keV}} \right)^{\alpha_T} \quad (8)$$

where A_{13} is the normalization at $10^{13} h^{-1} M_\odot$ in units of 10^{-6} and α_{M_g} is the slope of the SZ- M_g relation. Similarly, A_5 is the normalization at 5 keV in units of 10^{-5} and α_T is the slope of the SZ- T_m relation. The Table 2 lists the values of the best-fit normalization and slope measured at different radii for the $z=0$ sample. The errorbars shown in the Figure indicate 2σ confidence region of the best-fit slope and normalization in the CSF runs at each epoch.

The Figure shows that both SZ- M_g and SZ- T_m relations are as equally tight as the SZ-M relation. The best-fit slopes of the adiabatic runs are in very good agreement

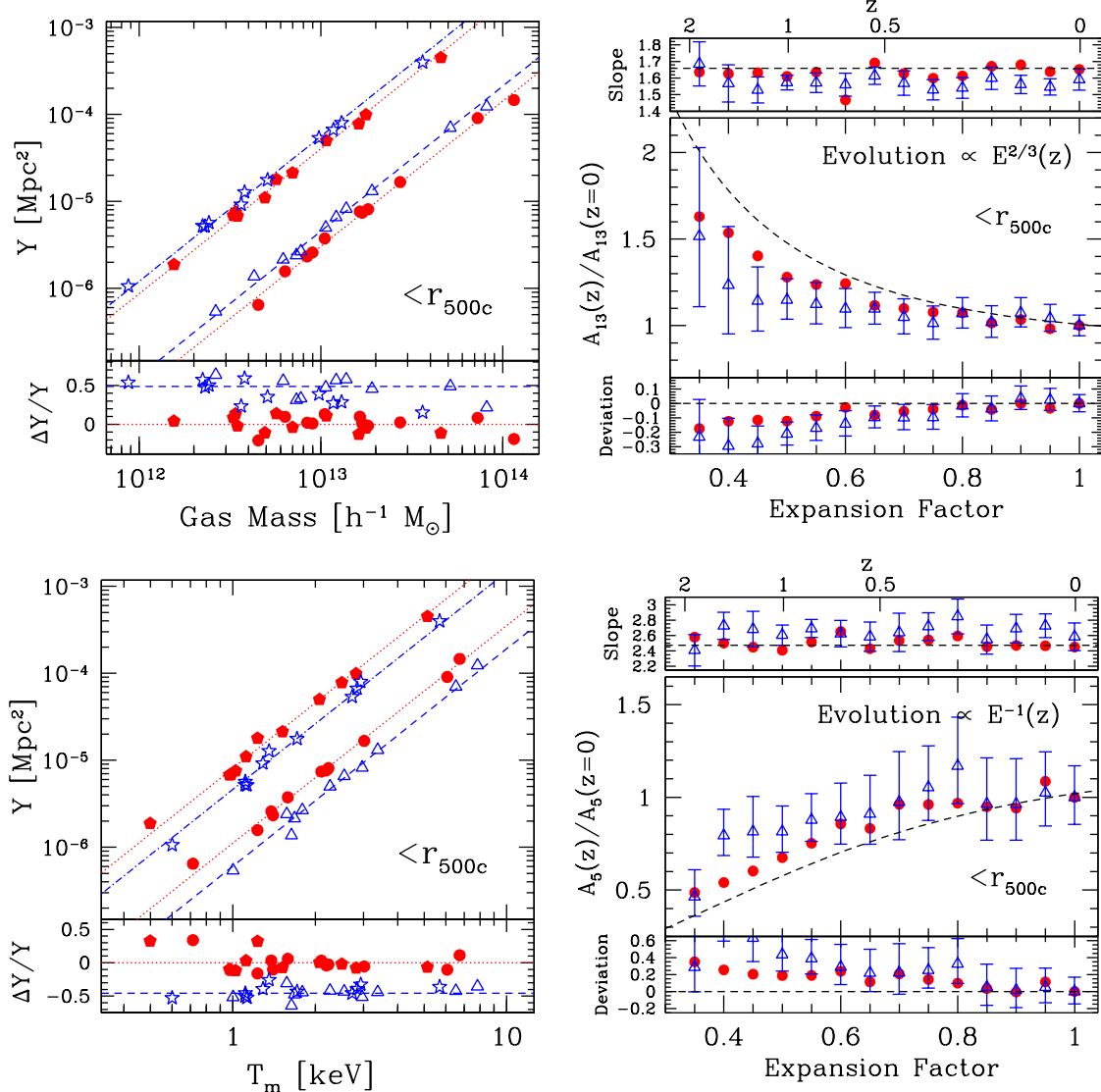


FIG. 6.— *Top panels:* the SZ flux-gas mass relations. The *left panel* shows the scaling relations at $z=0$ (bottom lines and points) and 1 (top lines and points). The *right panel* shows the redshift evolution of the slope and normalization between $z=2$ and 0 . The errorbars indicate 2σ confidence region of the best-fit slope and normalization in the CSF runs at each epoch. Point and line types are the same as in Fig. 3. *Bottom panels:* the relation between the SZ flux and the mass weighted temperature.

with the predicted slope of the self-similar model. The best-fit slopes of the CSF runs, on the other hand, are marginally consistent with the predicted slope, and there are indications that the slopes in the CSF run may be slightly smaller (larger) for the SZ- M_g (SZ- T_m) relations. We also find that the slope is constant with time in both the adiabatic and CSF runs.

While the tightness and the slopes of these relations are relatively unaffected, gas cooling and star formation have a large impact on their normalization. Figure 6 shows that the normalization of the CSF run is higher by 49% in the SZ- M_g relation at r_{500c} , while it is lower by 39% in the SZ- T_m relation at the same radius. Note that the change in the normalization of the SZ- M_g relation has opposite sign from the change in the SZ- M relation, because gas cooling and star formation significantly reduce the gas mass of the cluster. Recall that the inclusion of gas cooling and star formation reduces the

SZ signal by 29% and M_g by 35% at r_{500c} . For the slope of $5/3$, the decrease in M_g by 35% in the x-direction corresponds to the increase of the normalization by a factor of two. Combined with the reduction of the SZ signal, the net effect is the increase of the normalization by 49% at r_{500c} . Similar accounting works for the SZ- T_m relation as well. We also find that the impact of galaxy formation on the normalization becomes larger in the inner region of the cluster.

In contrast to the SZ- M relation, we find that the inclusion of gas cooling and star formation modifies the redshift evolution of the normalization in the SZ- M_g and SZ- T_m relations. In the CSF run, we find that the normalization of the SZ- M_g relation is systematically lower by $\approx 20\%$ at $z=1$ than the predicted normalization of the self-similar evolution model, while the SZ- T_m relation is higher by $\approx 40\%$ at $z=1$. The departure from the predicted evolution is mainly due to the evolution in f_{gas}

and T_m , not the SZ signal, as discussed above (see also the Figure 5). Note also that the redshift evolution of the adiabatic simulations is consistent with the self-similar model at all redshift within the errors.

4.3. Comparisons to Previous Work

We now compare the results of our simulations to the previous studies in the literature (White et al. 2002; da Silva et al. 2004; Motl et al. 2005). So far, all of the previous studies have used a large number of clusters extracted from large box cosmological simulations. While these simulations provide good statistics, the resolution is inevitably limited to resolve relevant physical processes. The present work is on the other end of the spectrum: the resolution is high, but the statistics is low. In this sense, our work is complimentary to the previous studies.

Using the SPH simulations, da Silva et al. (2004) studied the SZ scaling relations in adiabatic simulations and re-simulations in which gas was allowed to cool or was pre-heated. These studies showed that both strong gas cooling and preheating modify the slope of the SZ-M relation. They find that the slope in the cooling run ($\alpha_M = 1.79$) was steeper than the slope of the adiabatic run ($\alpha_M = 1.69$) by about 0.1. More recently, Motl et al. (2005) used the large sample of clusters simulated using an eulerian AMR code and studied the SZ-M relation in the adiabatic run and three resimulations in which they added gas cooling, star formation and feedback one at a time. These studies showed that the slope in the simulations that include both cooling and star formation is very similar to the slope in the adiabatic run. Similar results are obtained using the simulations performed with the entropy conserving Gadget code with cooling, star formation and feedback (White et al. 2002). The results of our simulations are also consistent with these findings. Moreover, Motl et al. (2005) showed that the slope in the cooling only run is steeper than the slope in the adiabatic run by about 0.1, consistent with the results reported by da Silva et al. (2004).

In addition to the scatter and slope of the relation, da Silva et al. (2004) investigated their redshift evolution. They showed that the slope and normalization of the SZ-M relation evolve with redshift according to the the self-similar model out to $z=2$ in their adiabatic and cooling only run. Motl et al. (2005) also found similar results in all four sets of their simulations up to $z=1.5$. We reached the same conclusions using the high-resolution simulations.

In summary, the scatter, slope and redshift evolution of the SZ observable-mass relation are generally insensitive to the details of the cluster gas physics. These results appear to be very robust. In fact, the agreement among different studies is rather remarkable, because these simulations were carried out using very different numerical techniques, resolution and implementation of various physical processes incorporated in the simulations.

Despite the robustness of the results discussed so far, the impact of galaxy formation on the normalization of the SZ flux-mass relation is not yet well understood, because the magnitude of the effect is closely related to the cold baryon fractions, which have not yet converged among different simulations. da Silva et al. (2004), for example, find that the normalization of the SZ-M re-

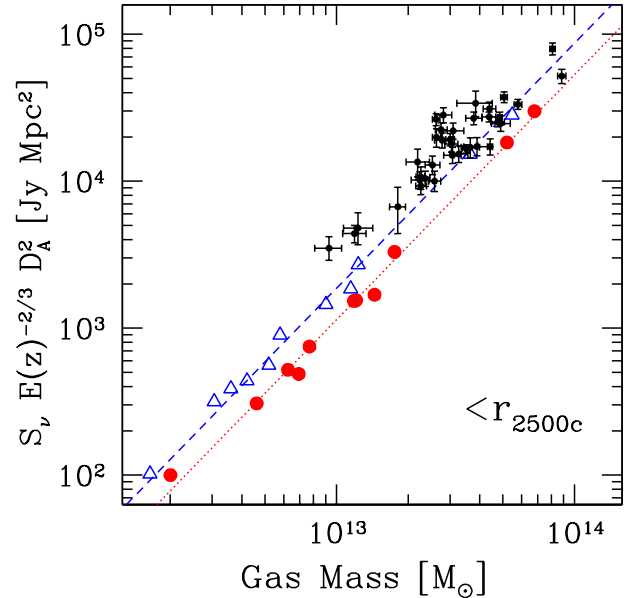


FIG. 7.— Comparisons of the SZ flux-gas mass relations in the simulations and observations. The *data points with errorbars* show the BIMA/OVRO SZ+Chandra X-ray cluster observations for a sample of 36 clusters (LaRoque 2005). The SZ flux is the integrated flux within the 2D projected aperture of R_{2500c} , while the gas mass is the enclosed gas mass within the sphere of r_{2500c} . The SZ flux is also corrected for the redshift evolution assuming the self-similar evolution model and the Λ CDM cosmology. The *solid circles* and *open triangles* show the eleven simulated clusters in the adiabatic and cooling and star formation runs, respectively, at $z=0$. The *dotted* and *dashed* lines are the best-fit relations at $z=0$ of each set of simulation. The figure shows that the simulations that include gas cooling and star formation are in reasonably good agreement with the data, while the adiabatic simulations are inconsistent with the observed relation.

lation in their cooling only run is lower by 20% and 9% at $M_{200c} = 10^{14}$ and $5 \times 10^{14} h^{-1} M_\odot$ compared to the adiabatic run, respectively. Moreover, White et al. (2002) discusses even smaller impact of galaxy formation in their simulation, because of the efficient energy feedback model used to regulate conversion of the hot gas into stars (Springel & Hernquist 2002). Using our high-resolution simulations, we report that gas cooling and associated star formation cause the decrease in the normalization of the SZ-M relation by 41, 34 and 32% at r_{2500c} , r_{500c} and r_{200c} , respectively, almost uniformly throughout the cluster mass range. This is one of the largest impacts on the SZ scaling relation reported to date.

4.4. Comparisons to Observations

To gauge how well the current simulations compare to the data, we compare the scaling relations in our simulations to the recent observational results. Figure 7 shows the comparisons of the SZ flux-gas mass relation from our simulations to the recent observational results based on the sample of 36 clusters observed with SZ BIMA/OVRO interferometers and Chandra X-ray telescope (LaRoque 2005). The cluster sample includes clusters in a broad redshift range from $z=0.14$ to $z=0.89$. For the comparison, we use the SZ flux-gas mass relation, rather than the SZ-total mass relation, because the gas mass can be mea-

sured more accurately using the Chandra X-ray cluster observations (see LaRoque 2005). The SZ flux is the integrated flux within the 2D projected aperture of R_{2500c} , while the gas mass is the enclosed gas mass within the sphere of r_{2500c} . These quantities are computed from the best-fit isothermal β model, fit jointly to the SZ and Chandra data (see LaRoque 2005, for details). The observed SZ flux at a given redshift is also corrected for the redshift evolution assuming the canonical self-similar model and the Λ CDM cosmology.

In the simulations, the SZ flux is computed by projecting the sphere of $3 \times r_{500c}$ centered around the minimum of the cluster potential. Note that the hot gas in the outskirts of the cluster makes non-negligible contribution to the SZ signal, if the projected aperture is a small fraction of the virial radius of the cluster. For the projected radius of R_{2500c} , we find that approximately 35% of the SZ signal arises from the region outside the sphere of r_{2500c} , on average. Although we find no systematic variation of the projection effect with the mass of the cluster, we find significant variation of the effect among different clusters at a level of about 20%. The contribution of the cluster outskirts becomes less significant as we make the projected aperture larger. The projection of the hot gas associated with the dense structures in the foreground or background of the cluster is not accounted for in this comparison.

The comparison shows that the simulations that include gas cooling and star formation are in reasonable agreement with the data, while the adiabatic simulations are inconsistent with the observed relation. This comparison therefore highlights the importance of galaxy formation in theoretical modelling of clusters and shows that the current generation of simulations produce clusters with gross properties similar to their observed counterparts.

5. DISCUSSION & CONCLUSIONS

We have presented the analysis of the Sunyaev-Zel'dovich (SZ) scaling relations using the high-resolution simulations of galaxy clusters formed in the concordance Λ CDM cosmology. The simulations of eleven individual clusters spanning a decade in mass ($M_{500c} = 3.5 \times 10^{13}$ to $9 \times 10^{14} h^{-1} M_\odot$) are performed with the shock-capturing eulerian adaptive mesh refinement N-body+gasdynamics ART code. We study the effects of gas cooling and star formation on the SZ scaling relations and their redshift evolution between $z=0$ and $z=2$ by comparing two sets of simulations performed with and without these processes included. The main results are summarized as follows.

1. The SZ signal integrated to sufficiently large fraction of the cluster volume correlates very strongly with the enclosed total cluster mass, independent of the details of the cluster physics or dynamical state of the cluster. The rms scatter of the SZ-total mass relation is about 10-15%.
2. The slope of the relation in the adiabatic run is in very good agreement with the predicted slope of the self-similar model in the entire probed redshift range. We find that the impact of the galaxy formation on the slope is small ($\lesssim 0.1$).

3. The redshift evolution of the SZ-total mass relation is consistent with the self-similar model between $z=0$ and $z=2$: (a) the slope is constant with redshift and (b) the normalization evolves with redshift according to the self-similar evolution model.
4. Gas cooling and star formation significantly modify the normalization of the SZ flux-total mass relation. The inclusion of these physical processes causes the decrease in the normalization of the relation by 41, 34 and 27% at r_{2500c} , r_{500c} and r_{180m} , respectively. The decrease is due to the large decrease in the gas fraction, which is offset somewhat by the increase in the mass weighted temperature. The baryon dissipation also causes the increase of the total cluster mass and hence modifies the normalization by a few percent.
5. The integrated SZ signal also correlates strongly with the gas mass and temperature of the clusters. The results (1)-(3) apply equally well for these scaling relations, except that the redshift evolution of the normalization exhibits deviation from the self-similar model increasing toward higher redshift. Gas cooling and star formation also significantly modify the normalization of these relations.
6. The SZ flux-gas mass relation in the simulations that include gas cooling and star formation is in reasonably good agreement with the observed relation recently obtained using the sample of 36 OVRO/BIMA SZ+Chandra X-ray observations (LaRoque 2005), while the simulations neglecting galaxy formation are inconsistent with the observed correlation.

These results have a number of important implications for the cosmological studies with the upcoming SZ cluster surveys. First and foremost, the SZ fluxes of clusters exhibit remarkable regularity at all redshifts, and the SZ signal integrated to sufficiently large fraction of the cluster volume is insensitive to the merging events (see e.g., Motl et al. 2005) or the properties of the cluster core (see § 4.1). This indicates that the integrated SZ flux is extremely good proxy for the total cluster mass. Second, we showed that the slope and redshift evolution of the relation are insensitive to the details of cluster gas physics, and they are well characterized by the simple self-similar cluster model between $z=0$ and 2. The simplicity of the redshift evolution of the slope and normalization implies that the self-calibration (Hu 2003; Majumdar & Mohr 2004) will be effective. Finally, these results appear to be very robust. In § 4.3, we showed that the same conclusions have been reached using the simulations with very different numerical techniques, resolution and implementation of various physical processes incorporated in the simulations.

Despite the simplicity of the redshift evolution, the normalization of the SZ flux-mass relation is much less understood, because the magnitude of the effect is closely related to the cold baryon fraction, which has not yet converged among different simulations. Using the high-resolution cluster simulations, we show that the radiative cooling and galaxy formation have significant impact on the normalization of the SZ scaling relations. In

our simulations, we find that the inclusion of gas cooling and star formation suppress the normalization by $\approx 30 - 40\%$, primarily due to the large reduction in the gas fractions. Interestingly, the SZ scaling relations in the simulations are in reasonably good agreement with the recent observational results. Moreover, the gas fractions in the simulations compare well with the measurements from deep Chandra X-ray observations of nearby clusters (Kravtsov et al. in preparation). Despite these successes in matching the SZ and X-ray observations, the current cluster simulations may still suffer from the "overcooling" problem since the fraction of baryons in the cold gas and stars within the virial radius of clusters at $z=0$ in our simulations is in the range 0.25-0.35, at least a factor of two higher than observational measurements (see Kravtsov et al. 2005, and references therein). In the simulations, the problem appears to be in the central brightest cluster galaxy, which contains a larger fraction of cluster stellar mass than is measured in observations. At the same time, the discrepancy may also be partly in the observed stellar fraction; for example, some fraction of cluster stellar mass in low-surface brightness intracluster component are missed in observations (e.g., Gonzalez et al. 2005; Lin & Mohr 2004).

Given the importance of these issues, further efforts from observers and theorists are needed to understand the SZ scaling relations to the level required for the cosmological studies. Observationally, it is important to increase the sample size and the number of low-mass clusters. Comparisons of different instruments will also help resolve systematic differences among different instruments (see e.g., Benson et al. 2004). It is also critical to understand the systematics in the measurements of the cluster mass through detailed and extensive comparisons of X-ray, SZ and optical cluster observations. With the advent of a number of dedicated SZ survey

instruments, the observational situation is expected to improve rapidly.

Theoretically, it is important to push the detailed theoretical modelling using the high-resolution cluster simulations to investigate the role of various processes, such as thermal conduction and AGN feedback, in suppressing cooling and star formation in cluster cores and their impact on the global properties of the cluster. For the cosmological application, it is also critical to understand the projection effects (White et al. 2002) and the nature of scatter in the observable-mass relation (Lima & Hu 2005). The high-resolution large box cluster simulations will likely provide important insights into these issues and help assess the effectiveness of the self-calibration technique (Hu 2003; Majumdar & Mohr 2004) in deriving the cosmological constraints from the future SZ cluster surveys.

I would like to thank Andrey Kravtsov and John Carlstrom for their invaluable guidance and advice during the course of this Ph.D. project. I would also like to thank Sam LaRoque for many useful discussions on the SZ observations and providing the data points for the comparisons with the simulations. I also thank Gus Evrard, Wayne Hu and Clem Pryke for useful comments and suggestions on the manuscript. This project was supported by the NASA Graduate Student Researchers Program and by NASA LTSA grant NAG5-7986. I also acknowledge the support from the Sherman Fairchild Foundation at Caltech, where the final revision to the manuscript was made. The cosmological simulations used in this study were performed on the IBM RS/6000 SP4 system (**copper**) at the National Center for Supercomputing Applications (NCSA).

REFERENCES

Benson, B. A., Church, S. E., Ade, P. A. R., Bock, J. J., Ganga, K. M., Henson, C. N., & Thompson, K. L. 2004, *ApJ*, 617, 829
 Bryan, G. L. & Norman, M. L. 1998, *ApJ*, 495, 80
 Carlstrom, J. E., Holder, G. P., & Reese, E. D. 2002, *ARA&A*, 40, 643
 Cooray, A. R. 1999, *MNRAS*, 307, 841
 da Silva, A. C., Kay, S. T., Liddle, A. R., & Thomas, P. A. 2004, *MNRAS*, 348, 1401
 Diaferio, A., Borgani, S., Moscardini, L., Murante, G., Dolag, K., Springel, V., Tormen, G., Tornatore, L., & Tozzi, P. 2005, *MNRAS*, 356, 1477
 Ferland, G. J., Korista, K. T., Verner, D. A., Ferguson, J. W., Kingdon, J. B., & Verner, E. M. 1998, *PASP*, 110, 761
 Gnedin, O. Y., Kravtsov, A. V., Klypin, A. A., & Nagai, D. 2004, *ApJ*, 616, 16
 Gonzalez, A. H., Zabludoff, A. I., & Zaritsky, D. 2005, *ApJ*, 618, 195
 Haardt, F. & Madau, P. 1996, *ApJ*, 461, 20
 Haiman, Z., Mohr, J. J., & Holder, G. P. 2001, *ApJ*, 553, 545
 Holder, G. P., Mohr, J. J., Carlstrom, J. E., Evrard, A. E., & Leitch, E. M. 2000, *ApJ*, 544, 629
 Hu, W. 2003, *Phys. Rev. D*, 67, 081304
 Kaiser, N. 1986, *MNRAS*, 222, 323
 Kennicutt, R. C. 1998, *ApJ*, 498, 541
 Klypin, A., Kravtsov, A. V., Bullock, J. S., & Primack, J. R. 2001, *ApJ*, 554, 903
 Kravtsov, A. V. 1999, PhD thesis, New Mexico State University
 Kravtsov, A. V., Klypin, A., & Hoffman, Y. 2002, *ApJ*, 571, 563
 Kravtsov, A. V., Nagai, D., & Vikhlinin, A. A. 2005, *ApJ*, 625, 588
 LaRoque, S. 2005, PhD thesis, University of Chicago
 Lima, M. & Hu, W. 2005, *Phys. Rev. D*, 72, 043006
 Lin, Y.-T. & Mohr, J. J. 2004, *ApJ*, 617, 879
 Majumdar, S. & Mohr, J. J. 2004, *ApJ*, 613, 41
 McCarthy, I. G., Babul, A., Holder, G. P., & Balogh, M. L. 2003, *ApJ*, 591, 515
 Metzler, C. A. 1998, unpublished ([astro-ph/9812295](#))
 Motl, P. M., Hallman, E. J., Burns, J. O., & Norman, M. L. 2005, *ApJ*, 623, L63
 Nagai, D. & Kravtsov, A. V. 2005, *ApJ*, 618, 557
 Navarro, J. F., Frenk, C. S., & White, S. D. M. 1996, *ApJ*, 462, 563
 —. 1997, *ApJ*, 490, 493
 Springel, V. & Hernquist, L. 2002, *MNRAS*, 333, 649
 Sunyaev, R. A. & Zeldovich, Y. B. 1970, *Comments on Astrophysics and Space Physics*, 2, 66
 —. 1972, *Comments on Astrophysics and Space Physics*, 4, 173
 Verde, L., Haiman, Z., & Spergel, D. N. 2002, *ApJ*, 581, 5
 Vikhlinin, A., Kravtsov, A., Forman, W., Jones, C., Markevitch, M., Murray, S. S., & V., S. L. 2005a, *ApJ* submitted ([astro-ph/0507092](#))
 Vikhlinin, A., Markevitch, M., Murray, S. S., Jones, C., Forman, W., & Van Speybroeck, L. 2005b, *ApJ*, 628, 655
 Voit, G. M. 2005, *Rev.Mod.Phys.*, 77, 207
 Voit, G. M. & Bryan, G. L. 2001, *Nature*, 414, 425
 Wang, L. & Steinhardt, P. J. 1998, *ApJ*, 508, 483
 Weller, J., Battye, R. A., & Kneissl, R. 2002, *Physical Review Letters*, 88, 231301
 White, M., Hernquist, L., & Springel, V. 2002, *ApJ*, 579, 16